Reversible metal-insulator transition of Ar-irradiated $LaAlO_3/SrTiO_3$ interfaces

P. P. Aurino,[1,*] A. Kalabukhov,[1] N. Tuzla,[2] E. Olsson,[2] A. Klein,[3] P. Erhart,[2] Y. A. Boikov,[4] I. T. Serenkov,[4] V. I. Sakharov,[4] T. Claeson,[1] and D. Winkler[1]

[1]*Department of Microtechnology and Nanoscience–MC2, Chalmers University of Technology, SE-412 96 Gothenburg, Sweden*
[2]*Department of Applied Physics, Chalmers University of Technology, SE-412 96 Gothenburg, Sweden*
[3]*Technische Universität Darmstadt, Fachbereich Material- und Geowissenschaften, 64287 Darmstadt, Germany*
[4]*Ioffe Physico-Technical Institute, Russian Academy of Sciences, St. Petersburg, Russia*

(Received 13 July 2015; published 19 October 2015)

The conducting state of a quasi-two-dimensional electron gas (q2DEG), formed at the heterointerface between the two wide-bandgap insulators $LaAlO_3$ (LAO) and $SrTiO_3$, can be made completely insulating by low-energy, 150-eV, Ar^+ irradiation. The metallic behavior of the interface can be recovered by high-temperature oxygen annealing. The electrical transport properties of the recovered q2DEG are exactly the same as before the irradiation. Microstructural investigations confirm that the transition is not due to physical etching or crystal lattice distortion of the LAO film below its critical thickness. They also reveal a correlation between electrical state, LAO film surface amorphization, and argon ion implantation. The experimental results are in agreement with density functional theory calculations of Ar implantation and migration in the LAO film. This suggests that the metal-insulator transition may be caused by charge trapping in the defect amorphous layer created during the ion irradiation.

DOI: 10.1103/PhysRevB.92.155130 PACS number(s): 73.40.−c, 79.60.Jv, 71.15.Mb, 73.90.+f

I. INTRODUCTION

The formation of a quasi-two-dimensional electron gas (q2DEG) has been reported when at least 4 unit cells (u.c.) of $LaAlO_3$ (LAO) are epitaxially grown on top of a $SrTiO_3$ (STO) substrate with a TiO_2 termination [1]. The interface shows interesting phenomena [2,3], including two-dimensional superconductivity [4,5], giant electric field effect [6], and magnetic ordering [7,8].

The mechanism of the q2DEG formation at the LAO/STO interface has been widely debated but an exact mechanism has not yet been revealed [9–14]. The polar catastrophe model has been proposed to relieve the electrostatic potential that is built up in the growing LAO film [15,16]. This model is in good agreement with the observation of a 4-u.c. critical thickness for the LAO film [4,6] but fails to explain a large number of other observations. Another possible mechanism is the doping due to oxygen vacancies at the free surface once a thickness of 4 u.c. is exceeded. The importance of oxygen vacancies has been emphasized in many studies [17–20]. Oxygen vacancies are produced in the STO substrate during the growth of the LAO film, and such defects are known to give electrical conductivity in STO [21]. Therefore, postannealing in oxygen atmosphere is critical to remove most of the oxygen vacancies. It has also been suggested that strain or interdiffusion can play a role [22]. Only recently a model based on first-principles calculations has been proposed that appears to provide the most comprehensive rationale [14]. It argues that various experimental observations (including, e.g., critical thickness, 2DEG density, and interface magnetism at both n-type and p-type interfaces) originate from an intricate balance of surface and interface defects, most importantly antisites as well as oxygen and lanthanum vacancies.

Significant efforts have been devoted to develop suitable techniques for patterning the q2DEG at the interface to fabricate prototype electronic devices, e.g., field effect transistors [23–28]. Ion bombardment is widely used for creating nanostructured surfaces by implantation, defect creation, and physical etching. It is, however, also known to create a few-nanometers-thick metallic layer at the surface of the STO substrate [18,29–31]. This is associated with formation of oxygen vacancies in the STO, each of them donating two conducting electrons. There have been several studies regarding the possibility of inducing a metal-insulator transition in the LAO/STO system by other methods. For example, an electric field has been applied to 3-u.c.-thick LAO to tune the conductivity [6]. Another possibility is to use an AFM tip to apply a voltage at the surface of a 3-u.c. insulating LAO film in order to make it metallic and metastable; the insulating state can then be recovered by applying an opposite voltage [32]. Ar ion etching was also used to etch the LAO film below the critical thickness [33]. The metallic state in this case could be recovered by deposition of LAO on the etched sample, but the electrical properties of the recovered state were not the same as in the original state.

In a previous work [34], we found that the electrical conductivity at the LAO/STO interface can be eliminated by short-time, low-energy Ar^+ irradiation. In our experiments, the initially conducting LAO/STO interface becomes insulating after only a few minutes of irradiation. The use of low energy and short irradiation time is crucial to avoid formation of oxygen vacancies in the bulk STO substrate donating conduction electrons and shunting the interface electrical properties. We also demonstrated that the use of low energy and small dose of irradiation does not result in a substantial physical etching of the film below its critical thickness. The effect, in conjunction with optical or e-beam lithography, was used to obtain a robust and reliable technique to pattern nanostructures down to 50 nm. However, the exact mechanism of the metal-insulator transition (MIT) induced by Ar^+ irradiation is still not understood.

In this work, we find that the metallic state can be completely restored through a high-temperature oxygen anneal of the irradiated sample. The electrical properties of irradiated

*aurino@chalmers.se

 ©2015 American Physical Society

and postannealed interface are strikingly similar to those of the original, as-grown interface. Importantly, the electrical mobility of the recovered sample is the same as before irradiation. This means that defects that are created during irradiation, and that lead to additional scattering, are completely healed upon high-temperature oxygen annealing. We discuss possible mechanisms of an induced metal-insulator transition by Ar ion beam irradiation in connection with different models explaining the formation of an electron gas in LAO/STO.

II. METHODS

LAO films were grown to 10-u.c.-thick layers on $5 \times 5\,\text{mm}^2$ large TiO_2-terminated STO [35,36] substrates using pulsed laser deposition (PLD) [37] with a laser energy density of $1.5\,\text{J/cm}^2$ and a laser spot area on the target of $2\,\text{mm}^2$. The substrate was heated to $800\,^\circ\text{C}$ in an oxygen pressure of 10^{-4} mbar during the deposition. The process was monitored using *in situ* reflection high-energy electron diffraction (RHEED) [38] that showed clear intensity oscillations confirming a layer-by-layer growth. Immediately after the deposition, the samples were annealed for 1 h at $600\,^\circ\text{C}$ and 500 mbar of pure oxygen. All the samples were inspected in an atomic force microscope (AFM, Bruker Dimension ICON) to confirm the smoothness of the surfaces and the presence of 1-u.c.-high step terraces.

After the deposition of the LAO film, each $5 \times 5\,\text{mm}^2$ sample was cut into two pieces of $5 \times 2.5\,\text{mm}^2$ using a Loadpoint Microace 3+ diamond saw. This allowed us to compare samples that had identical initial states before irradiation and postannealing. The surface of the LAO film was protected by a spin-coated polymer photoresist layer. AFM and electrical measurements showed that surface morphology and electrical transport properties were not affected by the cutting process.

The Ar^+ ion irradiation experiments were performed in an Oxford IonFab 300 Plus system using an inductively coupled plasma Ar^+ source and 3-cm beam aperture. A beam energy of 150 eV and a current density of $0.03\,\text{mA/cm}^2$ were used. The angle of the incident beam was set to 0° or 30° relative to the sample surface normal; where not otherwise specified the angle used is always 30°.

One of the two halves was irradiated by low-energy Ar^+ ions for 5 min. The irradiated sample showed a completely insulating behavior ($R > 200\,\text{G}\Omega$, measurement limit). The nonirradiated sample was metallic with values of sheet resistance $R_s \approx 10^5\,\Omega/\square$ and carrier density $n_s \approx 1.5 \times 10^{13}\,\text{cm}^{-2}$ at room temperature, characteristic of the LAO/STO interface [1].

The annealing of samples was performed in the same chamber used for the PLD, in order to be able to evaluate the crystalline quality of the surface *in situ* by RHEED at different temperatures during the process.

Electrical transport properties were measured in a four-point van der Pauw configuration using a Quantum Design PPMS system. Electrical contacts were provided by direct bonding of AlSi wire to the corners of the samples.

To reveal details regarding the atomic structure, high-angle annular dark-field (HAADF) scanning transmission electron microscopy (STEM) analysis of the interfaces was performed. For this purpose a FEI Titan 80–300 TEM/STEM with a probe Cs corrector was used at a voltage of 300 kV. Further investigations were performed using STEM energy-dispersive x-ray spectroscopy (EDX), a technique that makes use of a small convergent beam allowing chemical analysis at a local scale. Size of the probe is approximately 1 Å; it was used to investigate distinct points on the film and the substrate in different areas of the samples.

Medium-energy ion scattering (MEIS) using He^+ ions, with incident energy $E_0 = 93\,\text{keV}$, backscattering angle 120°, and electrostatic analyzer, was used to investigate the composition and crystal structure of LAO/STO samples. All measurements were performed at room temperature in an ultrahigh-vacuum chamber having a residual pressure of less than 10^{-7} mbar. When the ion beam axis is set to 8° to a low-index crystalline direction, which in our case coincides with the substrate normal, it is in a so-called random (or nonchanneling) mode. Scattered ions lose energy depending on the atomic weight of scatterers and on how far they have to straddle back to the surface. Thus, the scattered peak (or edge) intensity and energy provide information about the type and amount of scattering atoms as well as their location. Simulated spectra give numerical values as described in [39]. In the aligned (or channeling) mode, the incident ions are along the surface normal (crystal direction). They would be scattered only by atoms close to the surface in an ideal crystal as top atoms in the lattice columns shadow deeper-lying atoms. The scattered intensity peak should be sharper and more surface sensitive than in the random mode. Analysis of the spectra in both modes can, therefore, provide information regarding the film structure (relative to the ideal one) and the amounts of La and Al in the cationic sublattice.

Following reports on the implantation of Ar in insulating thin Al_2O_3 films [40], the samples were investigated using x-ray photoelectron spectroscopy (XPS) in order to check whether the Ar-irradiation process results in Ar implantation in the LAO film. The measurements were carried out with a Physical Electronics PHI 5700 system, which is equipped with a monochromatic Al $K\alpha$ x-ray source. The energy resolution, which is determined using the Gaussian broadening of the Fermi edge emission of sputter cleaned Ag foil is 0.4 eV. The binding energies of the same Ag foil were used for energy calibration of the spectra for the conducting samples. Insulating, ion-irradiated samples were measured with charge neutralization using an electron flood gun. All samples were measured as received without any chemical or temperature treatment.

To elucidate the properties of interstitial Ar in LAO, calculations were carried out within density functional theory (DFT) using the projector augmented wave formalism [41,42] as implemented in the Vienna *ab initio* simulation package [43,44]. The generalized gradient approximation as parametrized by Perdew, Burke, and Ernzerhof (PBE) [45] was employed to represent exchange and correlation effects. The $DFT + U$ method [46] was applied to correctly describe La $4f$ states using the same parameters as used previously for other La compounds [47,48]. Defect calculations were carried out using a $3 \times 3 \times 3$ supercell containing 135 ± 1 atoms. The Brillouin zone was sampled using a $2 \times 2 \times 2$ Monkhorst-Pack k-point mesh. As the defects considered are charge neutral, finite size and band gap corrections are very small as discussed extensively in Ref. [49], which also

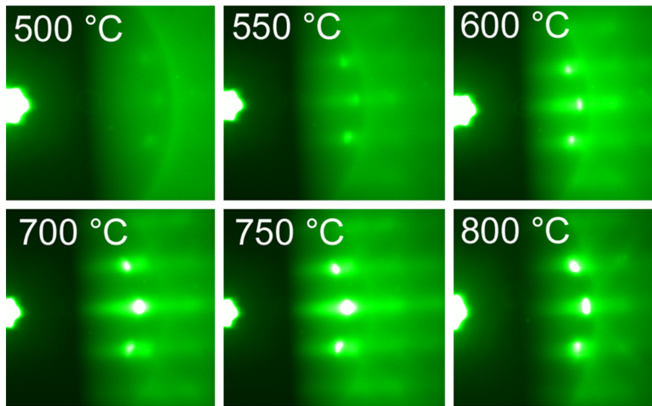

FIG. 1. (Color online) RHEED image of an irradiated 10-u.c. LAO film at different temperatures during the oxygen annealing process. The images are taken while the sample is heated at the rate of 40 °C per minute, in an oxygen pressure of 10^{-4} mbar. The interference pattern shows that the surface starts to recrystallize around 500 °C and is completely recrystallized at 600 °C. No further big change is seen up to 800 °C.

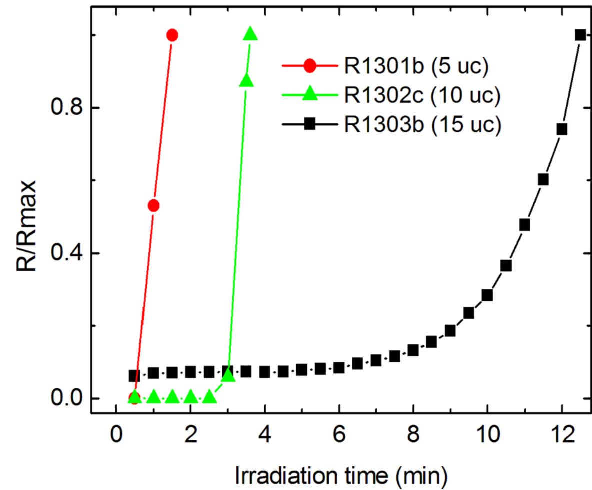

FIG. 3. (Color online) Electrical resistance of 5-, 10-, and 15-u.c. LAO/STO samples as a function of irradiation time measured *in situ* during the Ar ion irradiation at room temperature. The ion beam energy was 150 eV and 0° angle. The resistance is normalized to the maximum value.

provides additional information concerning the relevant defect thermodynamics. Formation volumes and formation volume tensors were computed from the cell metrics of the fully relaxed defect and ideal cells [50,51]. Migration barriers were obtained using the climbing image nudged elastic band method [52].

III. EXPERIMENTAL RESULTS

Figure 1 shows a series of *in situ* RHEED images of the 30° irradiated sample during the annealing process at 10^{-4} mbar of oxygen partial pressure at successively higher temperature during heating. At room temperature, the sample surface is amorphous as no RHEED pattern is seen. The recrystallization process begins at around 500 °C and the RHEED image shown in Fig. 1 corresponding to 600 °C is the same as for the LAO film after deposition (not shown). The RHEED pattern does not significantly change between 600 °C and 800 °C.

Irradiated samples annealed for 15 min at 800 °C in 10^{-4} mbar O_2 showed metallic behavior with conductivity and carrier concentration very similar to nonirradiated ones. The temperature dependencies of sheet resistivity, charge carrier density, and charge mobility for a sample that was irradiated and annealed at 800 °C (with postannealing for 1 h at 600 °C, 500 mbar O_2) and for a nonirradiated sample (postannealed similarly) are presented in Fig. 2. The mobility does not change noticeably. The carrier density of the annealed irradiated sample is slightly lower than that of the nonirradiated one at low temperature, but shows an upturn at around 30 K, surpassing the nonirradiated one. This may be due to the fact that the thickness of the sample is slightly reduced after irradiation. It is important to stress that the electrical properties of the LAO/STO interface can slightly change from sample to sample, but for each irradiated sample the annealing process restores a state equivalent to the respective original one. A similar behavior is observed for samples irradiated both at 30° and 0° angle of incidence.

To investigate the possible effect of oxygen pressure during the post annealing of the irradiated samples, different oxygen pressures were used during annealing at 800 °C; ranging from 10^{-4} to 10^{-1} mbar O_2. The annealing at 800 °C was followed by an additional annealing step of 1 h, at 600 °C and 500 mbar O_2, in every case. The conductivity was restored to the metallic

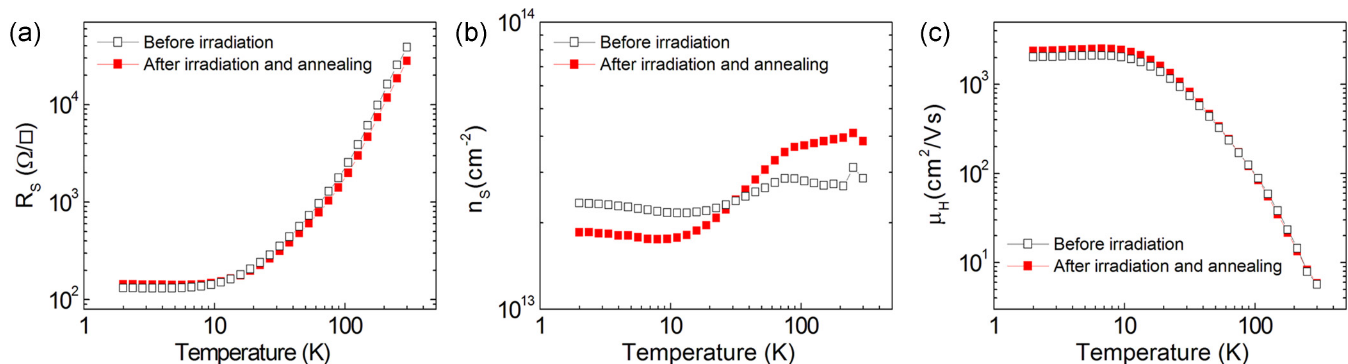

FIG. 2. (Color online) Temperature dependence of (a) sheet resistance, (b) carrier density, and (c) charge mobility for a 10-u.c. LAO/STO sample, just after the deposition and after being irradiated by 150-eV Ar^+, 0° angle, for 5 min and reannealed at 800 °C.

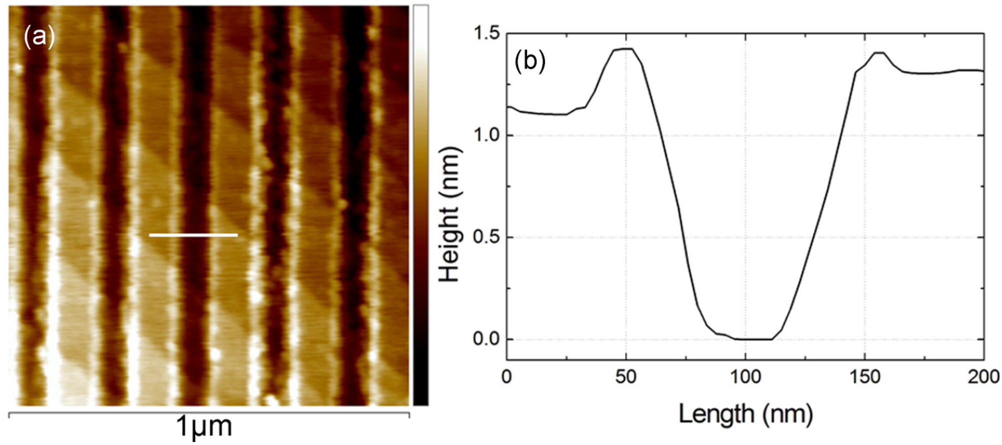

FIG. 4. (Color online) (a) (Color online) AFM image of a 10-u.c. LAO/STO sample patterned with 100-nm-wide nanostrips; the white line corresponds to the section profile. (b) Section profile height of the irradiated area; the step is only 1 nm.

state (as before irradiation) in all samples regardless of the oxygen partial pressure used.

We also investigated the time dependence of the resistance during low-energy ion beam irradiation for samples with different LAO film thickness. Three samples with thicknesses of nominally 5, 10, and 15 u.c. were irradiated under similar conditions as described above at 150 eV beam voltage, 0° incident beam, and their resistance was measured as a function of irradiation time *in situ*. The results are shown in Fig. 3. The measurement shows that the time required to reach the insulating state increases with the film thickness; the conductivity disappears after only 1 min of irradiation in the 5-u.c.-thick film, after 2 min for the 10-u.c.-thick film, and after 10 min for the 15-u.c.-thick film.

Thanks to our patterning technique [34], we were able to fabricate nanostrips with widths down to 50 nm. An AFM image of a sample patterned with 100-nm-wide strips is shown in Fig. 4, where the dark regions are the irradiated ones. The image shows that the difference of height between irradiated and nonirradiated areas is around 1 nm, corresponding to 2–3 u.c. decrease in height for the irradiated region. This sample was irradiated under 30° angle very close to maximum yield with respect to the etching rate [53]; in case of 0° angle irradiation, the step is much smaller and indistinguishable by AFM, as explained in [34]. HAADF STEM images of this sample, showing side-by-side irradiated and nonirradiated regions (as well as a transition region between these), are displayed in Fig. 5. They demonstrate that the topmost part of the irradiated LAO film is amorphous (or possibly covered by debris from the STEM sample preparation stage), while a crystalline part remains. Its thickness is always above the critical thickness of 4 u.c. STEM EDX mapping was performed on both areas of the (nanopatterned) samples that had been irradiated and areas protected from the ion beam, respectively

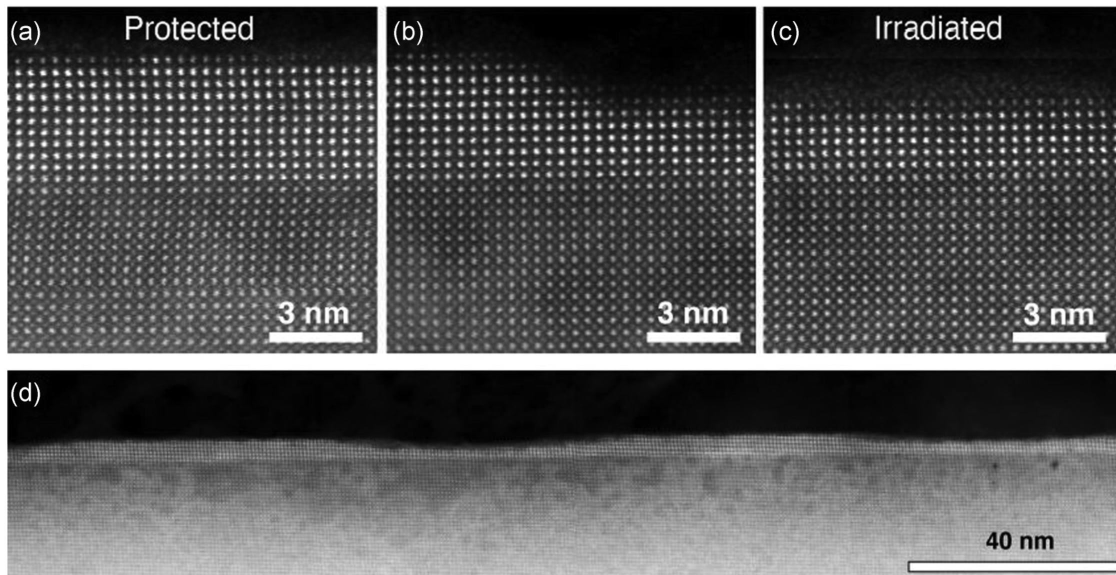

FIG. 5. HAADF STEM cross-section images of the 10-u.c.-thick patterned LAO film on STO substrate. (a) shows the protected part of the sample, with all 10 u.c. remaining, (b) shows the edge between the protected and the irradiated part, (c) shows the irradiated part of the sample, with uniform 5–6 u.c. of the crystalline LAO film visible, and (d) shows an overview of the patterned film, where several irradiated regions are visible.

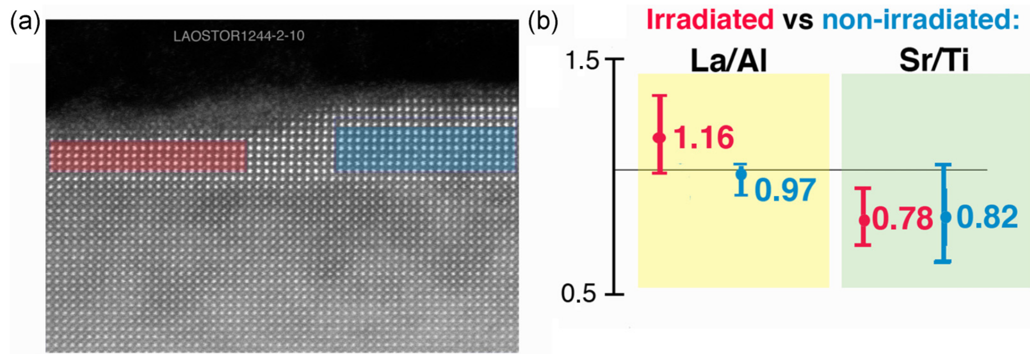

FIG. 6. (Color online) Representation of the acquired data collected with EDX. (a) Representative part of the irradiated (left) and nonirradiated (right) part of the film. Red and blue regions show examples of areas used for the acquisition of the STEM EDX data. (b) is a visualization of the collected data, gathered in one diagram. Diagram shows the La/Al and Sr/Ti ratio; each spot corresponds to the average ratio of irradiated (red) or nonirradiated (blue) area.

(see Fig. 6 for the definition of probed regions). Virtually all irradiated areas show La-rich compositions suggesting selective sputtering or segregation of Al (the latter was not seen by STEM). Care was taken to probe areas of the film with the same distance from the interface in both irradiated and nonirradiated regions. Statistical evaluation of the La/Al ratio was performed in this way. It repeatedly revealed a clear difference in stoichiometry between the irradiated and protected areas of the film. The results shown in Fig. 6 indicate that the La/Al ratio in a nonirradiated LAO film is, on average, 0.97. This is very close to the expected value of 1.00 (well within the error of the measurement) and agrees with the claims by [54] that the La/Al ratio has to be 1 or slightly below this value in order to form a conductive 2DEG. On the other hand, the same value for the irradiated parts of the film is 1.16. This information indicates Al depletion within the film as a consequence of the irradiation process. The ratio of Sr/Ti atoms that have diffused into the LAO during the deposition remains about the same before and after irradiation. As the amount of diffused atoms is much smaller than the host ones, the uncertainty in the measurement is larger, but the result indicates that Ti ions do not appreciably fill Al vacancies.

Figure 7(a) shows random and aligned MEIS spectra from an irradiated 10-u.c.-thick LAO sample (30°, 5 min). The aligned La peak height is only slightly smaller than the random one, indicating that the LAO film is, at least partially, amorphized. On the other hand, a Sr peak from the substrate does not appear in the aligned spectrum. This indicates effective shielding by a top crystalline La sublattice. Modeling of random and aligned spectra shows that about 60% of the top LAO film is amorphous; the rest of the film is crystalline. The equivalent thickness of the film obtained from numerical simulations is 5.4 u.c. Figure 7(b) shows random and aligned MEIS spectra from an irradiated and postannealed 10-u.c.-thick LAO sample. It shows that the amplitude of the aligned peak is much lower than the random one. This indicates a high crystalline quality of the material. Modeling of the random peak shows that it corresponds to an LAO film thickness of 7–8 u.c. This suggests that the film was completely recrystallized after postannealing. (The reason why the random La peak is much higher in a reannealed sample is not clear. It may be caused by sample thickness inhomogeneity but this is rather unlikely according to the AFM, STEM, and XPS data. The MEIS measurements were repeated two times on the same

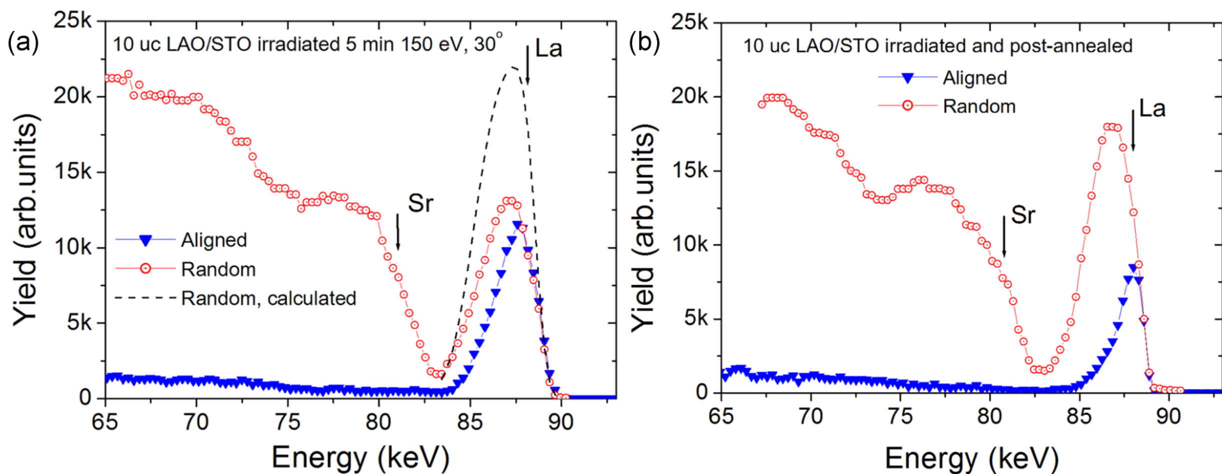

FIG. 7. (Color online) Random (open circles) and aligned (solid triangles) MEIS spectra of irradiated (a) and irradiated and postannealed (b) LAO/STO samples. Dashed line shows simulated random peak for stoichiometric 10-u.c.-thick LAO film. Similar heights of random and aligned La peaks for irradiated sample indicate an increased disorder of crystal lattice.

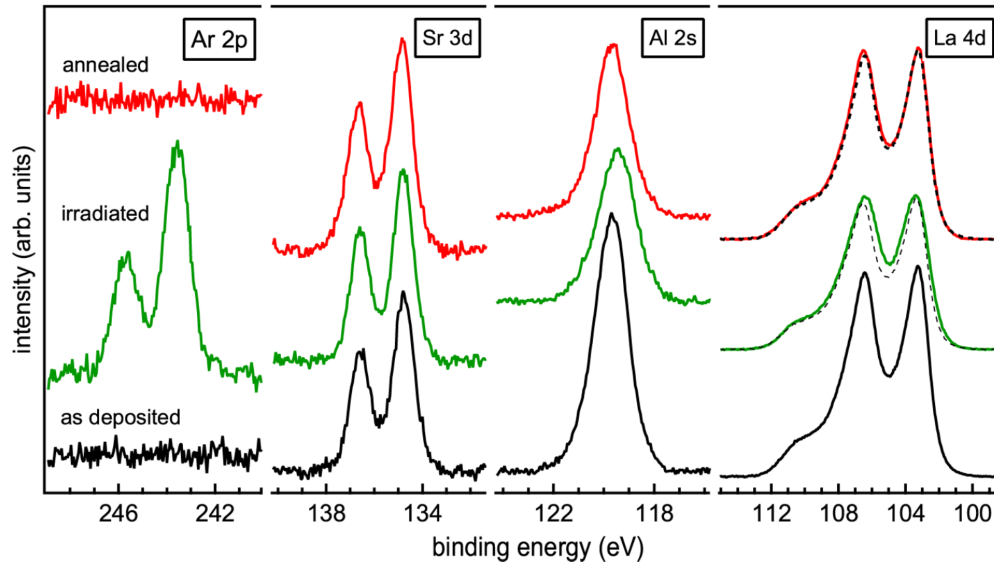

FIG. 8. (Color online) X-ray photoelectron spectra of STO/LAO samples after deposition and oxygen annealing (conducting), after Ar irradiation (insulating), and after Ar irradiation and reannealing (conducting). The La 4*d* spectrum of the as-grown sample is compared to the spectra of the irradiated and reannealed sample (dashed lines). The spectra of the irradiated sample have been shifted in order to match the binding energies of the conducting samples. Irradiation was performed at 30° incident angle.

sample with different energy of He ions; both gave identical results).

X-ray photoelectron spectra acquired from STO/LAO samples after deposition and oxygen annealing, after Ar irradiation, and after Ar irradiation and reannealing are shown in Fig. 8. The as-deposited and reannealed samples are conducting. The Ar-irradiated sample was insulating and charging during the measurement. In order to compensate the charging, the spectra of this sample were recorded using an electron flood gun. The flood gun parameters were adjusted to reveal high-resolution spectra rather than to reproduce the binding energies of the conducting samples. This resulted in binding energies of the Ar-irradiated samples, which are approximately 2 eV higher than those of the conducting samples. The spectra in Fig. 8 are offset by this value for better comparison. The linewidth of the Sr 3*d* spectra of the Ar-irradiated sample is comparable to those of the conducting samples, indicating a homogeneous surface potential.

The XPS spectra reveal a series of information about the Ar-irradiation process. Firstly, the Ar-irradiated sample clearly shows an Ar 2*p* emission, indicating the implantation of the species. The Ar signal disappeared after reannealing. Secondly, the signal intensity of the Sr 3*d* emission is almost the same for all three samples. This confirms that the LAO film thickness does not change significantly after Ar irradiation. Thirdly, the Al 2*s* intensity, more specifically, the Al 2*s*/La 4*d* intensity ratio is noticeably decreased after Ar irradiation. Finally, in contrast to the Al 2*s* peak, the La 4*d* peak of the irradiated sample is broadened compared to the peaks of the two conducting samples. The latter cannot be related to a charging issue, as the Sr 3*d* and Al 2*s* peaks do not show comparable effects. The broadening of the La 4*d* spectra of the insulating sample is rather related to the amorphization of the $LaAlO_3$ surface region. That the amorphization affects primarily the La 4*d* emission is likely, as the complex shape of the La 4*d* is determined by multiplet splitting related to charge transfer processes of the photoexcited state [55,56], which depends on the crystallographic and electronic structure.

IV. DISCUSSION

We have shown that the metallic interface between LAO and STO can be made insulating by low-energy Ar^+ irradiation. The process is fully reversible: Oxygen annealing at high temperature completely recovers a metallic state at the interface. All our experimental results indicate that the electrical properties of the as-grown interface, and the recovered ones after irradiation, are indistinguishable. The electrical conductivity and the mobility are exactly the same; see Fig. 2. The recovered conductivity survives anneals at high temperature in oxygen atmosphere, similar to as-deposited interfaces. The recovery of the metallic interface does not depend on the partial oxygen pressure during annealing.

We also prove that the MIT is not caused by physical etching or amorphization of the LAO film below the critical thickness, and that the remaining part of crystalline LAO is always above 4 u.c. AFM also shows that the LAO is never etched below critical thickness. RHEED shows that the LAO film surface is completely amorphized after irradiation. The crystalline structure is quickly recovered during the annealing process at temperatures above 500 °C (see Fig. 1). It is possible that the irradiated film is amorphized down to a remaining crystalline part that is less than the critical thickness, causing MIT assuming a polar catastrophe model. Upon annealing, the crystalline structure may be recovered and the interface becomes metallic again. However, TEM data of the irradiated samples indicate that the LAO film is amorphized only in the top few unit cell layers and that crystallinity in the bottom layers is not affected by the ion irradiation (see Fig. 5). This is further supported by MEIS data indicating that the bottom part of the film is still crystalline, and by XPS measurements showing that the films thickness is not

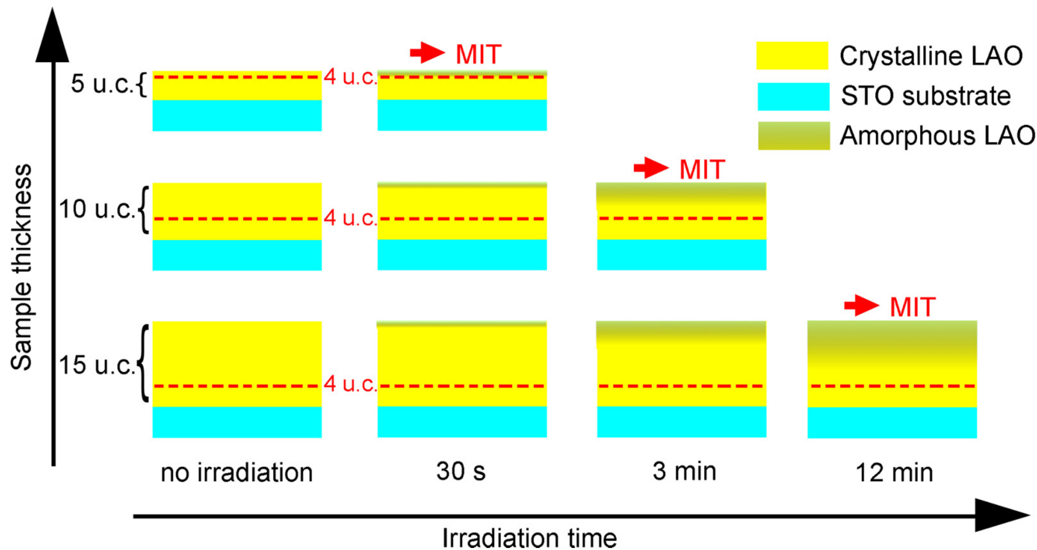

FIG. 9. (Color online) Schematic illustration of the effect of the irradiation on samples with different thickness. Irradiation causes amorphization of the top layer in the LAO film due to an increased concentration of implanted Ar. The probability of ions to penetrate deeper increases with the ion dose; therefore the thickness of the amorphous layer also increases.

decreased after irradiation. Based on this, we can rule out the possibility that MIT is related to a critical thickness effect in the LAO/STO interface.

It is also evident that the MIT is not related to any surface-induced damage only, since longer irradiation is required to eliminate conductivity in thicker LAO films (Fig. 3). The penetration depth is mainly defined by the energy of the ions. However, the probability of ions to penetrate deeper increases with the ion dose. Therefore, the longer the irradiation time, the deeper the penetration of the Ar^+ ions into the LAO/STO. Ar ions are likely to reach some distance in proximity to the interface in order to destroy the conductivity and therefore surface effects can be ruled out. This is illustrated schematically in Fig. 9.

STEM analysis indicates an increase in the La/Al ratio after irradiation. XPS measurements performed on samples after irradiation under a 30° angle also show a significant increase of the La/Al ratio (by a factor of 2), as compared to a nonirradiated LAO. It is reasonable to expect preferential sputtering of Al due to smaller mass mismatch to Ar. It is known that a metallic state of the LAO/STO interface requires a La/Al ratio slightly below 1 to provide compensation of La vacancies [54]. However, the electrical conductivity should not be recovered after annealing if Al atoms have been physically removed from the LAO film. Indeed, XPS data also showed that the La/Al ratio did not change after the irradiated sample was annealed and metallic conductivity was restored. Therefore, the change in the La/Al ratio cannot explain the observed metal-insulator transition.

Ion bombardment induces compositional, chemical, and structural changes in solid materials, depending on mass and energy. The energy of incoming ions can dissipate via elastic collisions with nuclei and via inelastic electronic excitations. The nuclear energy loss is dominant at low ion energies [57]. In our irradiation experiments, energy and time were chosen such that the penetration depth of the ions is only a few nanometers [34]. It is therefore unlikely that extended defects are created in the STO substrate that can cause carrier localization, as it was suggested for interfaces irradiated by high-energy protons [28]. The fact that oxygen vacancies are not induced in the STO substrate further proves that radiation-induced damage is mainly limited to a few top layers of the LAO film. A correlation between surface amorphization and presence of argon in the film, as indicated by XPS measurements, suggests that an amorphous LAO state may be stabilized by Ar implantation. Moreover, after thermal regrowth of the LAO film upon annealing above 600 °C, argon is released from the film.

To reconcile the experimental observations, we carried out density functional theory calculations as detailed in Sec. II concerning the properties of interstitial Ar in LAO. We considered three different interstitial sites including the octahedral site (surrounded by four O and two La atoms) and a tetrahedral site, as well as a low-symmetry configuration, in which an Ar and an O atom form a dumbbell-like configuration. The octahedral interstitial site, which corresponds to the largest open volume in the cubic perovskite structure, yields the lowest formation energy of 10.7 eV. This very large value arises because of the significant lattice strain that has to be accommodated and is also reflected in the large defect formation volume of 10.9 Å. The formation volume tensor indicates that the strain field associated with the defect is aligned along the La-Ar-La direction and exhibits considerable anisotropy with a factor of 2 between the largest and the two identical smaller eigenvalues [52]. While the incorporation of Ar is also possible at vacancy sites at a much smaller energy cost, the vacancy concentration is much smaller than the interstitial site density and will be quickly exhausted under irradiation conditions.

We considered several different pathways for Ar interstitial migration, the lowest of which has a barrier of 1.0 eV. Alternative pathways resulted in barriers in the range up to 1.7 eV. Based on the lowest barrier and the Einstein-Smoluchowski relation one can estimate the temperature above which this defect becomes mobile. Using typical

parameters for perovskite oxides [58], one finds that interstitial Ar is essentially immobile below a temperature of 500–600 K.

These findings suggest that after the implantation event, Ar remains in the material primarily in interstitial form. The interstitial is associated with a large formation volume causing significant lattice strain. As a result, one can expect that loading the LAO film with Ar destabilizes the perovskite lattice and triggers the transformation into an amorphous structure. The amorphous region features localized electronic states, similar to defect states in the case of a fully crystalline film, albeit at a much higher concentration. The localized states are known to enhance charge trapping in amorphous layers of various semiconducting and transition metal oxides [59–61]. It is also possible that an amorphous layer can cause accumulation of charges, resulting in a very strong potential across the film [62]. We have previously observed very strong electric fields in the Ar-irradiated LAO layers using Kelvin probe AFM [63].

The boundary between the crystalline and amorphous regions assumes the role of the surface in the model put forth by Yu and Zunger [14]. It is therefore pivotal for the observation of an MIT: The thickness of the amorphous top layer increases with irradiation time, shifting the amorphous-crystalline boundary (ACB) closer to the STO/LAO interface. Once the ACB is approximately within 4 u.c. of the interface the MIT occurs.

The detailed migration mechanism for Ar in amorphous LAO is naturally rather intricate. It is, however, reasonable to assume that the barriers obtained for crystalline material, which in the case of noble gases are largely determined by the open volume available in the lattice [49], are approximately indicative of the amorphous material as well, since the atomic densities are similar. It is then sensible that the mobility onset temperature estimated above of 500–600 K agrees rather well with the temperature, which is needed to reverse the MIT (and recrystallize the film) as this corresponds to the point at which Ar can leave the material again.

V. CONCLUSIONS

In conclusion, we demonstrate that low-energy Ar ion bombardment induces metal-insulator transition in the 2DEG formed at the interface between LAO and STO. We also show that the transition is fully reversible: Oxygen annealing at high temperature, surprisingly enough, completely recovers a metallic interface state that is identical to the original one. A combination of TEM, AFM, XPS, and MEIS studies indicated that the transition is not due to physical etching or damage of the film below its critical thickness. It also reveals correlation between electrical properties, surface amorphization, and Ar ion implantation. Density functional theory calculations suggest that Ar remains in the material primarily in interstitial form causing significant lattice strain. The onset of interstitial Ar migration is estimated at the temperature of 500–600 K, in good agreement with experimental observations. Therefore, the metal-insulator transition may be caused by charge trapping on defect states formed during the ion irradiation in the LAO film. Our results give insights into the physics of the LAO/STO interface and provide a tool for nanopatterning of devices on this basis.

ACKNOWLEDGMENTS

Valuable discussions with Professor P. Hyldgaard are greatly appreciated. We also appreciate M. Hagberg from the Nanofabrication Laboratory at Chalmers University of Technology for the help with ion beam etching. The work was supported by the Swedish Research Council, the Knut and Alice Wallenberg foundation, and the Swedish Institute Visby program. The support from the Swedish Infrastructure for Micro- and Nanofabrication–Myfab is appreciated. We acknowledge Project No. 15-02-03996 of the Russian Foundation for Basic Research.

[1] A. Ohtomo and H. Hwang, Nature **427**, 423 (2004).
[2] A. D. Caviglia, S. Gariglio, C. Cancellieri, B. Sacépé, A. Fête, N. Reyren, M. Gabay, A. F. Morpurgo, and J.-M. Triscone, Phys. Rev. Lett. **105**, 236802 (2010).
[3] A. D. Caviglia, M. Gabay, S. Gariglio, N. Reyren, C. Cancellieri, and J.-M. Triscone, Phys. Rev. Lett. **104**, 126803 (2010).
[4] N. Reyren, S. Thiel, A. D. Caviglia, L. Fitting-Kourkoutis, G. Hammer, C. Richter, C. W. Schneider, T. Kopp, A.-S. Räuetschi, and D. Jaccard, Science **317**, 1196 (2007).
[5] S. Gariglio, N. Reyner, A. D. Caviglia, and J.-M. Triscone, J. Phys.: Condens. Matter **21**, 164213 (2009).
[6] S. Thiel, G. Hammerl, A. Schmehl, C. W. Schneider, and J. Mannhart, Science **313**, 1942 (2006).
[7] L. Li, C. Richter, J. Mannhart, and R. Ashoori, Nat. Phys. **7**, 762 (2011).
[8] J. A. Bert, B. Kalisky, C. Bell, M. Kim, Y. Hikita, H. Y. Hwang, and K. A. Moler, Nat. Phys. **7**, 767 (2011).
[9] G. Herranz, M. Basletić, M. Bibes, C. Carrétéro, E. Tafra, E. Jacquet, K. Bouzehouane, C. Deranlot, A. Hamzić, J.-M. Broto, A. Barthélémy, and A. Fert, Phys. Rev. Lett. **98**, 216803 (2007).
[10] Z. S. Popović, S. Satpathy, and R. M. Martin, Phys. Rev. Lett. **101**, 256801 (2008).
[11] G. Herranz, F. Sànchez, N. Dix, M. Scigaj, and J. Fontcuberta, Sci. Rep. **2**, 758 (2012).
[12] H. W. Jang, D. A. Felker, C. W. Bark, Y. Wang, M. K. Niranjan, C. T. Nelson, Y. Zhang, D. Su, C. M. Folkman, S. H. Baek, S. Lee, K. Janicka, Y. Zhu, X. Q. Pan, D. D. Fong, E. Y. Tsymbal, M. S. Rzchowski, and C. B. Eom, Science **331**, 886 (2011).
[13] P. R. Willmott, S. A. Pauli, R. Herger, C. M. Schleputz, D. Martoccia, B. D. Patterson, B. Delley, R. Clarke, D. Kumah, C. Cionca, and Y. Yacoby, Phys. Rev. Lett. **99**, 155502 (2007).
[14] L. Yu and A. Zunger, Nat. Commun. **5**, 5118 (2014).
[15] R. Pentcheva and W. E. Pickett, Phys. Rev. Lett. **102**, 107602 (2009).
[16] N. Nakagawa, H. Y. Hwang, and D. A. Muller, Nat. Mater. **5**, 204 (2006).
[17] W. Siemons, G. Koster, H. Yamamoto, W. A. Harrison, G. Lucovsky, T. H. Geballe, D. H. A. Blank, and M. R. Beasley, Phys. Rev. Lett. **98**, 196802 (2007).
[18] A. S. Kalabukhov, R. Gunnarsson, J. Börjesson, E. Olsson, T. Claeson, and D. Winkler, Phys. Rev. B **75**, 121404 (2007).

[19] Y. Chen, N. Pryds, J. E. Kleibeuker, G. Koster, J. Sun, E. Stamate, B. Shen, G. Rijnders, and S. Linderoth, Nano Lett. **11**, 3774 (2011).
[20] A. Kalabukhov, Y. A. Boikov, I. T. Serenkov, V. I. Sakharov, J. Börjesson, N. Ljustina, E. Olsson, D. Winkler, and T. Claeson, Europhys. Lett. **93**, 37001 (2011).
[21] H. Frederikse, W. Thurber, and W. Hosler, Phys. Rev. **134**, A442 (1964).
[22] M. Huijben, A. Brinkman, G. Koster, G. Rijnders, H. Hilgenkamp, and D. H. A. Blank, Adv. Mater. **21**, 1665 (2009).
[23] J. Mannhart and D. G. Schlom, Science **327**, 1607 (2010).
[24] D. G. Schlom and J. Mannhart, Nat. Mater. **10**, 168 (2011).
[25] C. Schneider, S. Thiel, G. Hammerl, C. Richter, and J. Mannhart, Appl. Phys. Lett. **89**, 122101 (2006).
[26] N. Banerjee, M. Huijben, G. Koster, and G. Rijnders, Appl. Phys. Lett. **100**, 041601 (2012).
[27] S. Azimi, J. Song, C. J. Li, S. Mathew, M. B. H. Breese, and T. Venkatesan, Nanotechnology **25**, 445301 (2014).
[28] S. Mathew, A. Annadi, T. K. Chan, T. C. Asmara, D. Zhan, X. R. Wang, S. Azimi, Z. Shen, A. Rusydi, M. B. H. Breese, and T. Venkatesan, ACS Nano **7**, 10572 (2013).
[29] D. Kan, T. Terashima, R. Kanda, A. Masuno, K. Tanaka, S. Chu, H. Kan, A. Ishizumi, Y. Kanemitsu, and Y. Shimakawa, Nat. Mater. **4**, 816 (2005).
[30] H. Gross, N. Bansal, Y. Kim, and S. Oh, J. Appl. Phys. **110**, 073704 (2011).
[31] D. W. Reagor and V. Y. Butko, Nat. Mater. **4**, 593 (2005).
[32] C. Cen, S. Thiel, G. Hammerl, C. W. Schneider, K. E. Andersen, C. S. Hellberg, J. Mannhart, and J. Levy, Nat. Mater. **7**, 298 (2008).
[33] Z. Q. Liu, C. J. Li, W. M. Lü, X. H. Huang, Z. Huang, S. W. Zeng, X. P. Qiu, L. S. Huang, A. Annadi, J. S. Chen, J. M. D. Coey, T. Venkatesan, and Ariando, Phys. Rev. X **3**, 021010 (2013).
[34] P. P. Aurino, A. Kalabukhov, N. Tuzla, E. Olsson, T. Claeson, and D. Winkler, Appl. Phys. Lett. **102**, 201610 (2013).
[35] M. Kawasaki, K. Takahashi, T. Maeda, R. Tsuchiya, M. Shinohara, O. Ishiyama, T. Yonezawa, M. Yoshimoto, and H. Koinuma, Science **266**, 1540 (1994).
[36] G. Koster, B. L. Kropman, G. J. H. M. Rijnders, D. H. A. Blank, and H. Rogalla, Appl. Phys. Lett. **73**, 2920 (1998).
[37] D. B. Chrisey and G. K. Hubler, *Pulsed Laser Deposition of Thin Films* (John Wiley & Sons, New York, 1994).
[38] A. Ichimiya and P. I. Cohen, *Reflection High Energy Electron Diffraction* (Cambridge University Press, Cambridge, 2004).
[39] V. V. Afrosimov, R. N. Il'in, S. F. Karmanenko, A. A. Melkov, V. I. Sakharov, and I. T. Serenkov, Thin Solid Films **492**, 146 (2005).
[40] Y. Gassenbauer, A. Wachau, and A. Klein, Phys. Chem. Chem. Phys. **11**, 3049 (2009).
[41] P. E. Blöchl, Phys. Rev. B **50**, 17953 (1994).
[42] G. Kresse and D. Joubert, Phys. Rev. B **59**, 1758 (1999).
[43] G. Kresse and J. Hafner, Phys. Rev. B **47**, 558 (1993).
[44] G. Kresse and J. Furthmüller, Comput. Mater. Sci. **6**, 15 (1996).
[45] J. P. Perdew, K. Burke, and M. Ernzerhof, Phys. Rev. Lett. **77**, 3865 (1996); **78**, 1396(E) (1997).
[46] S. L. Dudarev, G. A. Botton, S. Y. Savrasov, C. J. Humphreys, and A. P. Sutton, Phys. Rev. B **57**, 1505 (1998).
[47] M. T. Czyzyk and G. A. Sawatzky, Phys. Rev. B **49**, 14211 (1994).
[48] D. Aberg, B. Sadigh, and P. Erhart, Phys. Rev. B **85**, 125134 (2012).
[49] P. Erhart, J. Appl. Phys. **111**, 113502 (2012).
[50] S. A. Centoni, B. Sadigh, G. H. Gilmer, T. J. Lenosky, T. Díaz de la Rubia, and C. B. Musgrave, Phys. Rev. B **72**, 195206 (2005).
[51] E. Jedvik, A. Lindman, M. Benediktsson, and G. Wahnström, Solid State Ionics **275**, 2 (2015).
[52] L. Gharaee and P. Erhart, J. Nucl. Mater. (2015).
[53] R. Behrisch, *Sputtering by Particle Bombardment* (Springer, Berlin, 1981).
[54] M. P. Warusawithana, C. Richter, J. Mundy, P. Roy, J. Ludwig, S. Paetel, T. Heeg, A. A. Pawlicki, L. F. Kourkoutis, L. F. Kourkoutis, M. Zheng, M. Lee, B. Mulcahny, W. Zander, Y. Zhu, J. Schubert, J. N. Eckstein, D. A. Muller, C. Hellberg, J. Mannhart, and D. G. Schlom, Nat. Commun. **4**, 2351 (2013).
[55] S. A. Chambers, M. H. Engelhard, V. Shutthanandan, Z. Zhu, T. C. Droubay, L. Quiao, P. Sushko, T. Feng, H. D. Lee, T. Gustafsson, E. Garfunkel, A. B. Shah, J.-M. Zuo, and Q. M. Ramasse, Surf. Sci. Rep. **65**, 317 (2010).
[56] C. Suzuki, J. Kawai, M. Takahashi, A.-M. Vlaicu, H. Adachi, and T. Mukoyama, Chem. Phys. **253**, 27 (2000).
[57] A. Benyagoub and L. Thomé, Phys. Rev. B **38**, 10205 (1988).
[58] P. Erhart and K. Albe, J. Appl. Phys. **102**, 084111 (2007).
[59] Y.-L. Wang, F. Ren, W. Lim, D. P. Norton, S. J. Pearton, I. I. Kravchenko, and J. M. Zavada, Appl. Phys. Lett. **90**, 232103 (2007).
[60] W. C. Wang, M. Badylevich, C. Adelmann, J. Swerts, J. A. Kitti, and V. V. Afanas'ev, IOP Conf. Ser.: Mater. Sci. Eng. **41**, 012008 (2012).
[61] E. M. F. Vieira, R. Diaz, J. Grisolia, A. Parisini, J. Martìn-Sànchez, S. Levichev, A. G. Rolo, A. Chahboun, and M. J. M. Gomes, J. Phys. D: Appl. Phys. **46**, 095306 (2013).
[62] O. Jbara, S. Fakhfakh, M. Belhaj, J. Cazaux, E. I. Rau, M. Filippov, and M. V. Adrianov, Nucl. Instrum. Methods Phys. Res., Sect. B **194**, 302 (2002).
[63] V. N. Popok, A. Kalabukhov, R. Gunnarsson, S. Lemeshko, T. Claeson, and D. Winkler, J. Adv. Microsc. Res. **5**, 26 (2010).